Clustering as Attention: Unified Image Segmentation with Hierarchical Clustering

Teppei Suzuki
Denso IT Laboratory, Inc.
suzuki.teppei@core.d-itlab.co.jp

Abstract

We propose a hierarchical clustering-based image segmentation scheme for deep neural networks, called *HCFormer*. We interpret image segmentation, including semantic, instance, and panoptic segmentation, as a pixel clustering problem, and accomplish it by bottom-up, hierarchical clustering with deep neural networks. Our hierarchical clustering removes the pixel decoder from conventional segmentation models and simplifies the segmentation pipeline, resulting in improved segmentation accuracies and interpretability. HCFormer can address semantic, instance, and panoptic segmentation with the same architecture because the pixel clustering is a common approach for various image segmentation. In experiments, HCFormer achieves comparable or superior segmentation accuracies compared to baseline methods on semantic segmentation (55.5 mIoU on ADE20K), instance segmentation (47.1 AP on COCO), and panoptic segmentation (55.7 PQ on COCO).[1]

1 Introduction

Image segmentation is a task of clustering pixels; for example, the semantic segmentation groups pixels that have the same semantics, and instance-level segmentation groups pixels in the same instance. However, many methods using deep neural networks define it as per-pixel classification tasks; for example, models for the semantic segmentation classify each pixel into pre-defined categories[37, 69, 8, 61], and models for the instance segmentation classify each pixel in the region of interest into foreground or background[20, 32, 16]. These classification approaches make the model architecture fragmented and task-specific because the classifier depends on the task definition, although recent studies[12, 11, 68] have attempted to design unified architectures that approach various segmentation tasks with the same architecture. Therefore, we revisit the segmentation architecture from the clustering perspective and investigate simpler, more interpretable architectures for unified image segmentation.

In general, segmentation models using neural networks consist of three parts: (i) a backbone model that aggregates spatial information, (ii) a pixel decoder that recovers the spatial resolution lost in the backbone, and (iii) a segmentation head that generates segmentation masks by a classifier or a cross-attention (or cross-correlation) between queries (or kernels) and feature maps. Existing segmentation heads can be interpreted as the pixel clustering modules (see Sec. 2.2). Thus, the segmentation pipeline of the models can be described as downsampling pixels in the segmentation head after upsampling them by using the pixel decoder because the clustering has the downsampling property. This pipeline would be somewhat redundant because for downsampling pixels (i.e., clustering in the segmentation head), the decoder upsamples pixels of the feature map already downsampled in the backbone. This insight provides the possibility of removing the pixel decoder: if downsampling layers in the backbone have the clustering property, we can remove the pixel decoder and achieve image

[1] Code: https://github.com/DensoITLab/HCFormer

Preprint. Under review.

segmentation by hierarchically grouping pixels at every downsampling layer and the segmentation head. However, the decoder is still needed to generate high-resolution masks because the obtained feature map from the backbone only presents downsampled, low-resolution 2D data.

To provide the clustering property for the downsampling layers, we propose a clustering module by interpreting the attention function[55] as a clustering solver and also propose a model using the proposed module, called *HCFormer*. HCFormer groups pixels at downsampling layers and realizes image segmentation by hierarchical clustering, as shown in Fig. 1. We attentively design the clustering module to be easily combined with existing backbone models (e.g., ResNet[21] and Swin Transformer[36]). As a result, our clustering module can be incorporated into the existing backbone models without a change in their feed forward path.

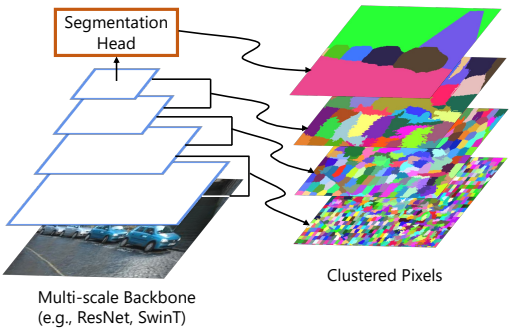

Figure 1: Overview of HCFormer. HCFormer hierarchically groups pixels at downsampling layers in the backbone and then groups clusters obtained from the backbone into an arbitrary number of clusters in the segmentation head.

Our clustering module simplifies the segmentation pipeline by removing the pixel decoder from conventional architectures. Instead of the pixel decoder, we upsample segmentation masks obtained from the segmentation head based on the clusters ontained from the backbone. While the models using the decoder must inherently solve an upsampling problem in addition to the segmentation problem, our model focuses only on the clustering problem because better clustering leads to better upsampling and segmentation masks. In HCFormer, the error in the upsampling process in the pixel decoder does not occur. Instead, the clustering error will occur, but it is possible to visualize and detect at which stage it occurs by seeing intermediate clustering results. We believe that this takes the segmentation model one step further in terms of interpretability.

Since pixel clustering is a common approach for various forms of image segmentation, HCFormer can approach many segmentation tasks in the same architecture. Thus, we evaluate HCFormer on three major segmentation tasks: semantic segmentation (ADE20K[70] and Cityscapes[13]), instance segmentation (COCO[35]), and panoptic segmentation (COCO[35]). HCFormer demonstrates comparable or better segmentation accuracy compared to the recent proposed unified models (e.g., MaskFormer[12] and K-Net[68]) and specialized models for each task, such as Mask R-CNN[20], SegFormer[61], and Panoptic FCN[31].

2 Method

In this section, we realize the hierarchical clustering in deep neural networks by providing a clustering property for downsampling layers. Simply, we may be able to do so by clustering pixels and then sampling representative values from obtained clusters, instead of conventional downsampling. However, the obtained clusters often do not form regular grid structures, and CNN-based backbones cannot compute data with irregular grid structures. Therefore, a straightforward approach, such as downsampling after clustering, is not applicable.

To incorporate the clustering procedure into existing backbone models while preserving data structures, we propose a *clustering-after-downsampling* strategy. We view downsampling used in existing backbone models as cluster-prototype sampling. Accordingly, we view the pixels in the feature map after downsampling as cluster prototypes, and group pixels in the feature map before downsampling. The proposed clustering module can be incorporated into existing backbones without altering their feed-forward path because it does not change downsampling procedure.

2.1 Attention as Clustering

We view the attention function[55] from the clustering perspective. Let $q \in \mathbb{R}^{C \times N_q}$ and $k \in \mathbb{R}^{C \times N_k}$ be a query and a key. N_q and N_k are the number of tokens for the query and key, and C denotes a

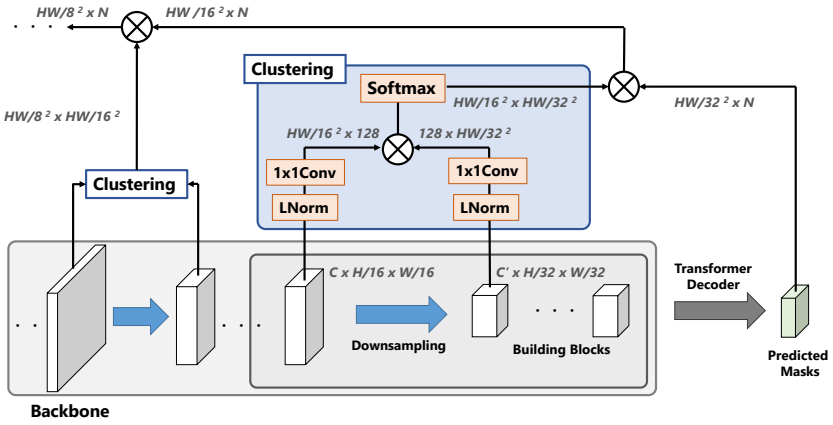

Figure 2: The computational scheme of our clustering module. We can view our clustering module as a variant of the attention module. LNorm and 1×1Conv denote layer normalization[2] and convolution with a kernel size of 1×1.

feature dimension. Then, the attention is defined as follows:

$$\text{Attention}(q, k; s) = \text{Softmax}_{\text{row}}(q^\top k/s), \tag{1}$$

where s denotes a scale parameter that is usually defined as $\sqrt{C}$. $\text{Softmax}_{\text{row}}(\cdot)$ denotes the row-wise softmax function. In general, the attention function is defined with a query, a key, and a value, but the value is omitted here for simplicity.

When $s \to 0$, eq. (1) corresponds to the following maximization problem:

$$\underset{A \in \{0,1\}^{N_q \times N_k}}{\arg\max} \langle A, q^\top k \rangle, \ s.t., \ \sum_j A_{ij} = 1, \tag{2}$$

where $\langle \cdot, \cdot \rangle$ denotes the Frobenius inner product. This maximization problem corresponds to the clustering problem for q with k as cluster prototypes. With an inner product as a similarity function, $A_{ij} = 1$ if q_i has the maximum similarity to k_j among all key tokens; otherwise, $A_{ij} = 0$. In other words, each row of A indicates the cluster index assigned to q_i, which is known as the assignment matrix. The attention in eq. (1) corresponds to a relaxed matrix of A obtained from eq. (2). Thus, we can view the attention, eq. (1), as the *soft* clustering for q.

2.2 Image Segmentation by Hierarchical Clustering

We show the computational scheme of the proposed clustering module in Fig. 2. For clustering, we obtain an intermediate feature map and its downsampled feature map from a backbone model. These are fed into layer normalization[2] and convolution layers with a kernel size of 1×1, as in the transformer block[55, 18]. We define the obtained feature maps as $F^{(i)} \in \mathbb{R}^{C_F \times \frac{H}{2^i} \frac{W}{2^i}}$ and $F_d^{(i)} \in \mathbb{R}^{C_F \times \frac{H}{2^{i+1}} \frac{W}{2^{i+1}}}$. C_F is the output channel of the 1×1 convolution, which is set to 128 in our experiment; H and W are the height and width of an input image; and $i \in \mathbb{N}$ is a scale factor of the spatial resolution that corresponds to the number of applied downsampling layers. We assume that the downsampling halves height and width respectively, and the ℓ_2-norm of the feature vector of each pixel is normalized as 1, which gives the inner product a perspective as the cosine similarity.

Then, the proposed clustering is defined as follows:

$$\text{Clustering}(F^{(i)}, F_d^{(i)}; s^{(i)}) = \text{Softmax}_{\text{row}}((F^{(i)})^\top F_d^{(i)}/|s^{(i)}|). \tag{3}$$

We define $s^{(i)} \in \mathbb{R}$ as a trainable parameter. As already described in Sec. 2.1, when $s^{(i)} \to 0$, eq. (3) corresponds to the clustering problem for $F^{(i)}$ with $F_d^{(i)}$ as cluster prototypes. Thus, we can provide the clustering property for the downsampling layers by computing eq. (3) after downsampling and accomplish the hierarchical clustering in deep neural networks, as shown in Fig. 1.

The obtained feature map from a backbone model (hereafter referred to as cluster features) is further clustered by the segmentation head used in [12], and segmentation masks are obtained. The cluster features are fed into the transformer decoder with trainable queries $Q \in \mathbb{R}^{C_q \times N_m}$, and the mask queries $\mathcal{E}_{\text{mask}} \in \mathbb{R}^{C_m \times N_m}$ are generated. The number of queries, N_m, is a hyperparameter. Note that the transformer "decoder" is different from the pixel decoder because one of its roles is to generate the mask queries, not to upsample the feature map. The cluster features are also mapped into the C_m-dimensional space by a linear layer, and we define them as $\mathcal{E}^{(i=5)}_{\text{cluster}} \in \mathbb{R}^{C_m \times \frac{H}{2^i} \frac{W}{2^i}}$. Then, the predicted masks are computed as follows:

$$M^{(i=5)} = \text{Sigmoid}(\mathcal{E}^{\top}_{\text{mask}} \cdot \mathcal{E}^{(i=5)}_{\text{cluster}}). \tag{4}$$

Note that we assume that the scale i is 5 because the conventional backbone has five downsampling layers. This segmentation head can also be viewed as the clustering, which groups $\frac{H}{2^i} \frac{W}{2^i}$ pixels in the cluster features into N_m clusters.[2]

The per-pixel classification head, which is the segmentation head used in many semantic segmentation models, can also be viewed from the clustering perspective. In the per-pixel classification head, the weight of the linear classifier with the softmax activation that produces class probability can be viewed as a set of class prototypes. The linear classifier groups pixels based on the class prototypes with the inner product as the similarity. Specifically, let $w \in \mathbb{R}^{C \times K}$ be a weight matrix of the linear classifier, which corresponds to the K-class prototypes with C-dimensional features, and let $f \in \mathbb{R}^{C \times M}$ be a feature map with M pixels. Then, the per-pixel classification models classify pixels as $\text{Softmax}_{\text{row}}(f^{\top} w)$, which is the same formula as the attention in eq. (1) (the norm of w can be viewed as the inverse of the scale parameter s). Therefore, we can also view this as the soft clustering problem and naturally incorporate our hierarchical clustering scheme into the per-pixel classification models. We evaluate our method using the per-pixel classification model in the Appendix.

2.3 Decoding

The obtained masks $M^{(i=5)} \in \mathbb{R}^{N_m \times \frac{H}{2^i} \frac{W}{2^i}}$ are low-resolution, and each spatial index corresponds not to a pixel but a cluster generated in the backbone by eq. (3). Thus, we have to decode it to obtain masks in the input image space. The decoding process is defined as follows:

$$\begin{aligned}(M^{(i)})^{\top} &= \text{Clustering}(F^{(i)}, F^{(i)}_d; s^{(i)})(M^{(i+1)})^{\top} \\ &= \text{Softmax}_{\text{row}}\left((F^{(i)})^{\top} F^{(i)}_d / |s^{(i)}|\right)(M^{(i+1)})^{\top},\end{aligned} \tag{5}$$

which corresponds to the attention function[55], although queries, keys, and values are obtained from different layers. From the hard clustering perspective, eq. 2, we can view the decoding as an operation of copying the cluster's representative value to its elements. Thus, this decoding process will be accurate if the each cluster is composed of pixels that are annotated with the same ground-truth label.

This cluster-based decoding allows us to remove the pixel decoder. Unlike the conventional pixel decoder, this decoding can be interpreted. In other words, it is possible to detect at which stage the error occurred by visualizing intermediate clustering results. In addition, the low-resolution feature maps are fed into the segmentation head because our decoding is applied after predicting masks. It contributes reduction of FLOPs in the segmentation head.

2.4 Efficient Computation

Let M be the number of pixels and then computational costs of the proposed clustering are $O(M^2)$, which is the same complexity as the common attention function[55], and it is intractable for high-resolution images. Various studies exist on reducing complexity[36, 47, 5, 62, 57, 54, 44], and we approach it with the local attention strategy.

We divide the feature map before downsampling, $F^{(i)}$, into 2×2 windows. The window size is determined by a stride of downsampling, which is assumed to be 2 in this paper. Each window

[2]The mask prediction uses the sigmoid function, not the softmax function. Thus, eq. (4) does not correspond to the clustering problem, eq. (2). However, in the post-processing, the mask that has the maximum confidence is selected as the prediction, meaning that the mask prediction including the post-processing corresponds to eq. (2). Further details can be found in the Appendix.

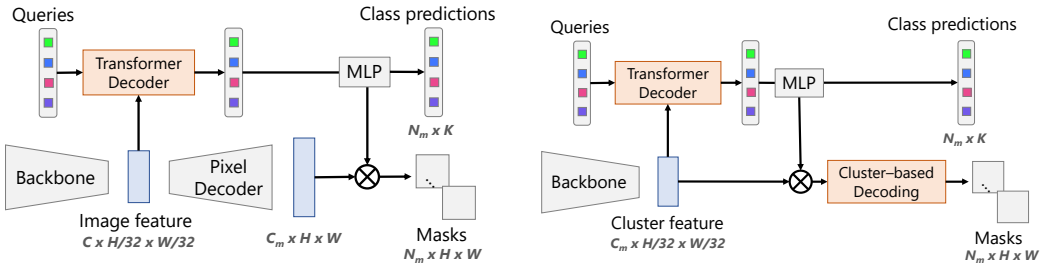

(a) MaskFormer (b) HCFormer

Figure 3: Comparison between MaskFormer[12] and HCFormer. MaskFormer upsamples a feature map and then predicts masks. In contrast, HCFormer directly predicts masks from downsampled feature maps. Instead of the pixel decoder, HCFormer recovers the resolution by cluster-based decoding, which corresponds to eq. (5).

corresponds to the pixel in the feature map after downsampling, $F_d^{(i)}$. Then, the attention is computed between a pixel in the window and the corresponding pixel in $F_d^{(i)}$ and its surrounding eight pixels, which is the same technique used in superpixel segmentation[24, 1] that is a pixel clustering algorithm. We illustrate this local attention in the Appendix. As a result, the complexity decreases to $O(M)$.

2.5 Architecture

We show an architecture of a baseline model, MaskFormer[12], and our model using the proposed clustering module in Fig. 3. The proposed model removes the pixel decoder from the baseline model and instead decodes the predicted masks using eq. (5). Optionally, we build a six-layer transformer encoder after the backbone, as in MaskFormer[12]. For class prediction, the mask queries are fed into multi-layer perceptrons and classified into K classes.

The flexibility of the downsampling is important because for our clustering module, the downsampled pixels are the cluster prototypes that should be representative values of clusters. However, unlike transformer-based backbones, the receptive field of CNN-based backbones is limited even if the deeper model is used[39, 61]. Thus, the CNN-based backbones may not sample effective pixels for the clustering module. To improve the flexibility, we replace downsampling layers (e.g., strided convolution) to which the proposed clustering module is attached with a deformable convolution v2[71] that deforms kernel shapes and modulates weight values. This replacement is only adopted for a CNN-based backbone. We verify its effect in the Appendix.

3 Experiment

3.1 Implementation Details

We implement our model on the Mask2Former author's implementation.[3] We use the transformer decoder with the masked attention[11], and the number of decoder layers is set to 8.

To train our model, we use the binary cross-entropy loss and the dice loss[40] as the mask loss: $\mathcal{L}_{\text{mask}} = \lambda_{\text{ce}}\mathcal{L}_{\text{ce}} + \lambda_{\text{dice}}\mathcal{L}_{\text{dice}}$. The training loss is a combination of mask loss, classification loss, and a L1 regularization term for $s^{(i)}$ in eq. (3): $\mathcal{L}_{\text{mask}} + \lambda_{\text{cls}}\mathcal{L}_{\text{cls}} + \lambda_{\text{reg}}\mathcal{L}_{\text{reg}}$, where $\mathcal{L}_{\text{cls}}$ is a cross-entropy loss and $\mathcal{L}_{\text{reg}} = \sum_i |s^{(i)}|$. λ_{reg} is set to 0.1. The regularization enforces the proposed attention-based clustering, eq. (3), to be the hard clustering, eq. (2). Following [11], we set $\lambda_{\text{ce}} = 5.0$, $\lambda_{\text{dice}} = 5.0$, and $\lambda_{\text{cls}} = 2.0$. As in [11], the loss is calculated with points for memory efficiency. Other training protocol is the same as for Mask2Former[11] (e.g., optimizer, its hyperparameters, and the number of training iterations). Additionally, the number of queries is the same as the Mask2Former setting. The details can be found in the Appendix.

[3] `https://github.com/facebookresearch/Mask2Former`

Table 1: Evaluation results for panoptic segmentation with COCO `val`. HCFormer+ stacks six-layer transformer encoder after the backbone, as in MaskFormer[12].

method	backbone	PQ	PQ^{Th}	PQ^{St}	AP^{Th}_{pan}	$mIoU_{pan}$	#params.	FLOPS
Panoptic FCN[31]	R50	44.3	50.0	35.6	-	-	-	-
MaskFormer[12]	R50	46.5	51.0	39.8	33.0	57.8	45M	181G
K-Net[68]	R50	47.1	51.7	40.3	-	-	-	-
Mask2Former[11]	R50	51.9	57.7	43.0	41.7	61.7	44M	226G
HCFormer	R50	47.7	51.9	41.2	35.7	59.8	38M	87G
HCFormer+	R50	50.2	55.1	42.8	38.4	60.2	46M	96G
MaskFormer[12]	Swin-S	49.7	54.4	42.6	36.1	61.3	63M	259G
Mask2Former[12]	Swin-S	54.6	60.6	45.7	44.7	64.2	69M	313G
HCFormer	Swin-S	50.9	55.7	43.6	38.9	63.1	62M	170G
HCFormer+	Swin-S	53.0	58.1	45.3	41.2	64.4	70M	183G
Max-Deeplab[56]	Max-L	51.1	57.0	42.2	-	-	451M	3692G
MaskFormer[12]	Swin-L	52.7	58.5	44.0	40.1	64.8	212M	792G
K-Net[68]	Swin-L	54.6	60.2	46.0	-	-	-	-
Mask2Former[11]	Swin-L	57.8	64.2	48.1	48.6	67.4	216M	868G
HCFormer	Swin-L	55.1	60.7	46.7	44.3	66.2	210M	715G
HCFormer+	Swin-L	55.7	62.0	46.1	45.3	66.4	217M	725G

We use the same post-processing as [12]: we multiply class confidence and mask confidence and use the output as the confidence score. Then, the mask with the maximum confidence score is selected as the predicted mask at each pixel.

The clustering module defined in eq. (3) is incorporated into every downsampling layer, except for those in the stem blocks of ResNet[21] and the patch embedding layer in Swin Transformer[36]. Thus, hierarchical level, namely the number of clustering modules, is 3.

3.2 Main Results

As baseline methods, we choose the recent proposed methods for unifying segmentation tasks, MaskFormer[12], K-Net[68], and Mask2Former[11] and specialized models for each task[31, 56, 61, 20]. We compare our method to the baselines with several backbones, ResNet-50[21], Swin-S[36], and Swin-L[36]. Note that ResNet-50 and Swin-S were pretrained with ImageNet-1K, and Swin-L was pretrained with ImageNet-22K. The training procedure and evaluation metrics are following [11]. We train models three times and report medians.

We first show the evaluation results for panoptic segmentation on the COCO validation dataset[35] in Tab. 1. HCFormer improves accuracies from the baseline model, MaskFormer. We consider that this is because the feature space of the feature map fed into the transformer decoder (hereafter referred to as the value vectors) is the similar to that of the cluster features, which compute the inner product with the mask query in eq. (4), in HCFormer. The mask queries obtained from the transformer decoder would have a similar feature to the value vectors because the cross-attention used in the transformer decoder basically computes a weighted sum of the value vectors. Thus, in HCFormer, the transformer decoder does not need to adjust the feature space of the value vectors to that of the cluster features, meaning that the task becomes simple and optimization would be made somewhat easy. In contrast, MaskFormer transforms the features nonlinearly by the pixel decoder, and hence the transformer decoder (or the pixel decoder) in MaskFormer has to adjust the feature space between the mask queries and the cluster features to predict the mask by eq. (4). Mask2Former improves accuracies from MaskFormer for the same reason, because the transformer decoder used in Mask2Former uses the intermediate feature maps obtained from the pixel decoder that contain the feature map close to the output layer (i.e., the cluster feature). In addition, the well-designed pixel decoder would refine the cluster features and drastically improve accuracies from MaskFormer.

HCFormer outperforms the other unified approach, K-Net[68], and the specialized models, Panoptic FCN[31] and Max-Deeplab[56], for all backbone models on panoptic segmentation. As shown in Tabs. 2 and 3 (a), HCFormer also outperforms MaskFormer, K-Net, and specialized models on instance segmentation with COCO and semantic segmentation with ADE20K[70]. In particular, HCFormer significantly improves AP^L from MaskFormer on instance segmentation. This would be because the pixel decoder in MaskFormer cannot accurately recover the large objects, whereas

Table 2: Evaluation results for instance segmentation with COCO `val`. HCFormer+ stacks six-layer transformer encoder after the backbone.

method	backbone	AP	AP^S	AP^M	AP^L	$AP^{boundary}$	#params.	FLOPs
Mask R-CNN[20]	R50	37.2	18.6	39.5	53.3	23.1	44M	201G
MaskFormer[12]	R50	34.0	16.4	37.8	54.2	23.0	45M	181G
Mask2Former[11]	R50	43.7	23.4	47.2	64.8	30.6	44M	226G
HCFormer	R50	37.4	16.7	40.0	59.7	24.6	38M	87G
HCFormer+	R50	40.1	18.8	43.0	62.3	26.9	46M	96G
Mask2Former[11]	Swin-L	50.1	29.9	53.9	72.1	36.2	216M	868G
HCFormer	Swin-L	46.4	24.1	50.5	70.9	32.6	210M	715G
HCFormer+	Swin-L	47.1	25.6	51.5	70.3	33.3	217M	725G

Table 3: Evaluation results for semantic segmentation with ADE20K and Cityscapes `val`. HCFormer+ stacks six-layer transformer encoder after the backbone.

(a) ADE20K

method	backbone	crop size	mIoU	FLOPs
MaskFormer[12]	R50	512	44.5	53G
Mask2Former[11]	R50	512	47.2	73G
HCFormer	R50	512	45.5	29G
HCFormer+	R50	512	46.9	32G
SegFormer[61]	MiT-B2	512	46.5	62G
MaskFormer[12]	Swin-S	512	49.8	79G
Mask2Former[11]	Swin-S	512	51.3	98G
HCFormer	Swin-S	512	48.8	56G
HCFormer+	Swin-S	512	50.1	58G
SegFormer[61]	MiT-B5	640	51.0	184G
MaskFormer[12]	Swin-L	640	54.1	375G
Mask2Former[11]	Swin-L	640	56.1	403G
HCFormer	Swin-L	640	55.2	338G
HCFormer+	Swin-L	640	55.5	342G

(b) Cityscapes

method	backbone	mIoU	FLOPs
MaskFormer[12]	R50	76.5	405G
Mask2Former[11]	R50	79.4	527G
HCFormer	R50	76.7	196G
HCFormer+	R50	78.3	225G
SegFormer[61]	MiT-B2	81.0	717G
MaskFormer[12]	Swin-S	78.5	599G
Mask2Former[11]	Swin-S	82.6	727G
HCFormer	Swin-S	79.3	398G
HCFormer+	Swin-S	80.0	427G
SegFormer[61]	MiT-B5	82.4	1460G
MaskFormer[12]	Swin-L	81.8	1784G
Mask2Former[11]	Swin-L	83.3	1908G
HCFormer	Swin-L	81.6	1578G
HCFormer+	Swin-L	82.0	1607G

such errors do not occur in HCFormer because it does not have the pixel decoder. In contrast, the performance for small objects, AP^S, is almost identical for both HCFormer and MaskFormer.

On Cityscapes[13] (Fig. 3 (b)), mIoU of HCFormer is worse than that of Segformer (that is the specialized model for semantic segmentation), although HCFormer improves mIoU from MaskFormer. Unlike COCO and ADE20K, the Cityscapes dataset contains only urban street scenes, and there are many thin or small objects, such as poles, signs, and traffic lights. MaskFormer and HCFormer do not have a pixel decoder or modules to capture such small and thin objects, and hence such objects would be missed in an intermediate layer.

For further analysis, we visualize intermediate clustering results and a predicted mask using HCFormer with Swin-L in Fig. 4. From the visualization of undersegmentation error, we find that the model groups pixels well except for the boundaries, but it misclassifies clusters for the small objects in this image (e.g., poles and person in the center). HCFormer cannot extract semantically discriminative features for such small objects, although the obtained features are discriminative in terms of the clustering. We believe that this analysis plays a role in interpretability, and conventional models do not allow for this type of analysis. We present further results and analysis on other datasets in the Appendix.

3.3 Ablation Study

To investigate the effect of the hierarchical level and the more effective architecture, we evaluate PQ, FLOPs, and the number of parameters of our model with various hierarchical levels and different numbers of transformer decoder layers. We use the COCO dataset and the ResNet-50 backbone for evaluation. We show an additional ablation study in the Appendix. The results are shown in Tabs. 4 and 5. PQ improves as both the hierarchical level and the number of decoder layers increase.

Since the resolution of the predicted masks also increases in line with the hierarchical level, the model can predict high-resolution masks. The hierarchical level of 2 would be preferred based on the

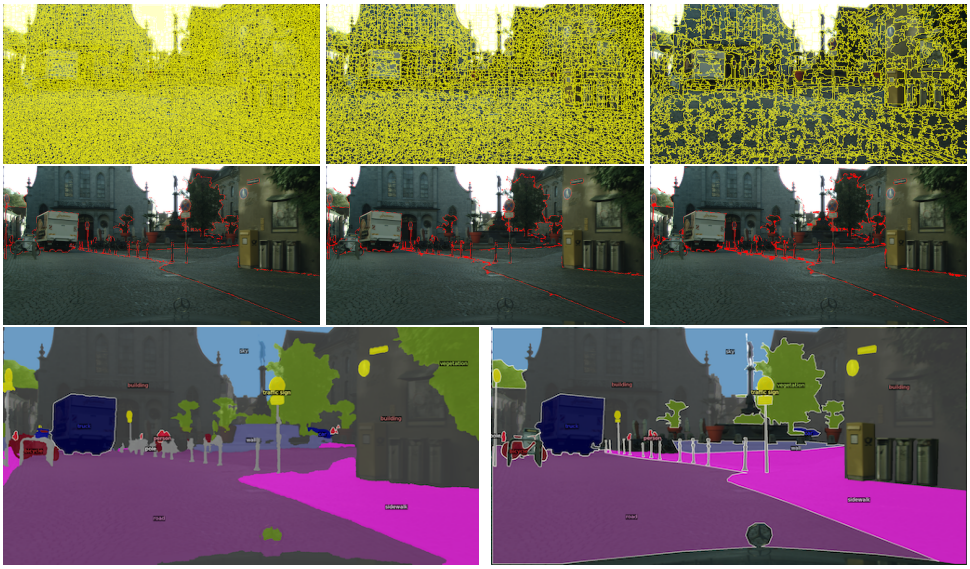

Figure 4: Hierarchical clustering results for Cityscapes. The top row shows the cluster boundaries, the middle row shows undersegmentation error[48] as red regions, which measures the "leakage" of clusters with respect to ground truth, and the bottom row shows a predicted mask (left) and a ground-truth label (right).

Table 4: Evaluation results for COCO `val`. with various hierarchical levels.

Hierarchical Level	0	1	2	3
PQ	41.9	45.6	46.7	47.7
FLOPs	82G	83G	84G	87G
#Params	37M	38M	38M	38M

Table 5: Evaluation results for COCO `val`. with various numbers of transformer decoder layers.

#Decoder Layers	1	2	4	8	16
PQ	42.0	44.8	46.7	47.7	48.0
FLOPs	85G	85G	86G	87G	90G
#Params	27M	29M	32M	38M	51M

balance between accuracy and computational costs in practice, although we adopt the hierarchical level of 3 in Sec. 3.2. In particular, PQ in our model is still comparable to that of the baseline model, MaskFormer[12], even when the hierarchical level is 2.

Our model does not work well with only one decoder layer, as with other models using the transformer decoder[12, 11, 6]. In terms of the balance between accuracy and computational costs, four or eight layers would be suitable for our model.

4 Related Work

4.1 Image Segmentation with Deep Neural Networks

Since FCNs[37] have been proposed, deep neural networks have become a de facto standard approach for image segmentation. As main segmentation tasks, semantic, instance, and panoptic segmentation are studied.

Semantic segmentation is often defined as per-pixel classification tasks, and various FCN-based methods have been proposed for semantic segmentation[69, 7, 3, 8, 9, 61]. In instance segmentation, many methods[20, 16, 33, 15, 32] depend on the object proposal, which is used for instance discrimination because instance segmentation has the object detection perspective. The pipeline of many proposal-based methods is somewhat complex, and thus proposal-free methods have been studied to simplify the pipeline, which uses the clustering approach including cross-attention (cross-correlation)[28, 41, 25, 17, 29, 58, 59]. Panoptic segmentation has been proposed in [27], which is a task combining semantic and instance segmentation. In early work, panoptic segmentation is approached with two separated modules for generating semantic masks and instance masks and then fusing them[27, 26, 10, 63]. To simplify the framework, Panoptic FCN[31] unifies the mod-

ules by using dynamic kernels. Panoptic FCN generates kernels from a feature map and produces segmentation masks by cross-correlation between the kernels and feature maps. As a similar approach, cross-attention with the transformer decoder is adopted in other panoptic segmentation methods[56, 6, 12, 11]. Such approaches also simplify the panoptic segmentation pipeline.

While many studies investigate task-specific modules and architectures, they cannot be applied models for other tasks. Thus, recent work investigates the unified architectures[12, 68, 11]. These methods use cross-attention-based approaches that can generate segmentation masks regardless of task definition. They have demonstrated effectiveness in the various segmentation tasks and have achieved comparable or better results compared to the specialized models. Our study also focuses on such unified architectures and builds our model based on MaskFormer[12], which is a unified approach.

Many studies on image segmentation focus on the segmentation head or the pixel decoder. In particular, various decoder architectures have been proposed, thereby improving segmentation accuracies[34, 43, 4, 46, 23, 30, 60, 9]. However, the decoder would make the segmentation problem complex: models using the decoder have to solve not only the segmentation problem but also the upsampling problem internally. Such models suffer from an error in the upsampling process of the pixel decoder. In addition, it is difficult to interpret whether the prediction error is due to upsampling or classification because upsampling is performed in the high-dimensional feature space.

The pixel decoder is not necessarily required for image segmentation with deep neural networks. In fact, FCN-32s[37], which is the simplest variant of FCNs, does not use the trainable decoder, although the generated masks are low-resolution and the segmentation accuracy is somewhat low. To keep the resolution in the backbone, several methods[7, 67, 69, 8] use dilated convolution[67, 7], which expands the convolution kernel by inserting holes between its consecutive elements, and replace the stride with the dilation rate. Such approaches can generate high-resolution masks, but the inference speed is very slow because the backbone must compute high-resolution feature maps.

4.2 Hierarchical Clustering

Hierarchical clustering approaches are sometimes used to solve image segmentation. For example, some previous methods[14, 19, 22, 52, 65, 66, 51, 50, 53, 45] group pixels into small segments by using superpixel segmentation[1, 49, 24] for pre-processing; the obtained segments are then merged or classified to obtain the desired cluster. Such a hierarchical approach often reduces computational costs and improves segmentation accuracy compared to directly clustering or classifying pixels.

A recent proposed method, called GroupViT[64], is a bottom-up, hierarchical clustering method. However, GroupViT is specialized for vision transformers[18] and for semantic segmentation with text supervision. In contrast, our method can be incorporated into most multi-scale backbone models, such as ResNet[21] and Swin Transformer[36], and used for arbitrary image segmentation tasks.

5 Conclusion

We proposed a method that introduces the clustering property into conventional downsampling layers in the deep neural networks. As a result, we accomplished image segmentation via hierarchical clustering in deep neural networks and simplified the segmentation pipeline by removing the pixel decoder used in many image segmentation models. In experiments, we verified that our method achieves comparable or better accuracies compared to baseline methods for semantic, instance, and panoptic segmentation. Since our hierarchical clustering allows visualization of the segmentation process, we believe that the hierarchical clustering not only simplifies the segmentation models but also enhances their interpretability.

Limitation. As described in the experimental section, the segmentation accuracies of our method are lower than the model using the well-designed pixel decoder[11]. While many findings exist for the pixel decoder to improve accuracy, no such finding has yet been made in our hierarchical clustering model. In addition, HCFormer basically has fewer FLOPs than the baseline model, MaskFormer, but the inference speed of HCFormer is not as fast as MaskFormer (about 10% slower) because the clustering module is not efficient compared to convolution used in the pixel decoder, even though the clustering module uses the local attention. Therefore, we will investigate more effective architectures or modules for the hierarchical clustering models in terms of latency and accuracy in future work.

References

[1] Radhakrishna Achanta, Appu Shaji, Kevin Smith, Aurelien Lucchi, Pascal Fua, and Sabine Süsstrunk. SLIC superpixels compared to state-of-the-art superpixel methods. *IEEE transactions on pattern analysis and machine intelligence*, 34(11):2274–2282, 2012.

[2] Jimmy Lei Ba, Jamie Ryan Kiros, and Geoffrey E Hinton. Layer normalization. *arXiv preprint arXiv:1607.06450*, 2016.

[3] Vijay Badrinarayanan, Alex Kendall, and Roberto Cipolla. Segnet: A deep convolutional encoder-decoder architecture for image segmentation. *IEEE transactions on pattern analysis and machine intelligence*, 39(12):2481–2495, 2017.

[4] Vijay Badrinarayanan, Alex Kendall, and Roberto Cipolla. Segnet: A deep convolutional encoder-decoder architecture for image segmentation. *IEEE transactions on pattern analysis and machine intelligence*, 39(12):2481–2495, 2017.

[5] Irwan Bello. Lambdanetworks: Modeling long-range interactions without attention. *arXiv preprint arXiv:2102.08602*, 2021.

[6] Nicolas Carion, Francisco Massa, Gabriel Synnaeve, Nicolas Usunier, Alexander Kirillov, and Sergey Zagoruyko. End-to-end object detection with transformers. In *European conference on computer vision*, pages 213–229. Springer, 2020.

[7] Liang-Chieh Chen, George Papandreou, Iasonas Kokkinos, Kevin Murphy, and Alan L Yuille. Deeplab: Semantic image segmentation with deep convolutional nets, atrous convolution, and fully connected crfs. *IEEE transactions on pattern analysis and machine intelligence*, 40(4):834–848, 2017.

[8] Liang-Chieh Chen, George Papandreou, Florian Schroff, and Hartwig Adam. Rethinking atrous convolution for semantic image segmentation. *arXiv preprint arXiv:1706.05587*, 2017.

[9] Liang-Chieh Chen, Yukun Zhu, George Papandreou, Florian Schroff, and Hartwig Adam. Encoder-decoder with atrous separable convolution for semantic image segmentation. In *Proceedings of the European conference on computer vision (ECCV)*, pages 801–818, 2018.

[10] Bowen Cheng, Maxwell D Collins, Yukun Zhu, Ting Liu, Thomas S Huang, Hartwig Adam, and Liang-Chieh Chen. Panoptic-deeplab: A simple, strong, and fast baseline for bottom-up panoptic segmentation. In *Proceedings of the IEEE/CVF conference on computer vision and pattern recognition*, pages 12475–12485, 2020.

[11] Bowen Cheng, Ishan Misra, Alexander G. Schwing, Alexander Kirillov, and Rohit Girdhar. Masked-attention mask transformer for universal image segmentation. *arXiv preprint arXiv:2112.01527*, 2021.

[12] Bowen Cheng, Alex Schwing, and Alexander Kirillov. Per-pixel classification is not all you need for semantic segmentation. volume 34, 2021.

[13] Marius Cordts, Mohamed Omran, Sebastian Ramos, Timo Rehfeld, Markus Enzweiler, Rodrigo Benenson, Uwe Franke, Stefan Roth, and Bernt Schiele. The cityscapes dataset for semantic urban scene understanding. In *Proc. of the IEEE Conference on Computer Vision and Pattern Recognition (CVPR)*, 2016.

[14] Camille Couprie, Clément Farabet, Laurent Najman, and Yann LeCun. Indoor semantic segmentation using depth information. *arXiv preprint arXiv:1301.3572*, 2013.

[15] Jifeng Dai, Kaiming He, and Jian Sun. Convolutional feature masking for joint object and stuff segmentation. In *Proceedings of the IEEE conference on computer vision and pattern recognition*, pages 3992–4000, 2015.

[16] Jifeng Dai, Kaiming He, and Jian Sun. Instance-aware semantic segmentation via multi-task network cascades. In *Proceedings of the IEEE conference on computer vision and pattern recognition*, pages 3150–3158, 2016.

[17] Bert De Brabandere, Davy Neven, and Luc Van Gool. Semantic instance segmentation with a discriminative loss function. *arXiv preprint arXiv:1708.02551*, 2017.

[18] Alexey Dosovitskiy, Lucas Beyer, Alexander Kolesnikov, Dirk Weissenborn, Xiaohua Zhai, Thomas Unterthiner, Mostafa Dehghani, Matthias Minderer, Georg Heigold, Sylvain Gelly, et al. An image is worth 16x16 words: Transformers for image recognition at scale. *arXiv preprint arXiv:2010.11929*, 2020.

[19] Clement Farabet, Camille Couprie, Laurent Najman, and Yann LeCun. Learning hierarchical features for scene labeling. *IEEE transactions on pattern analysis and machine intelligence*, 35(8):1915–1929, 2012.

[20] Kaiming He, Georgia Gkioxari, Piotr Dollár, and Ross Girshick. Mask R-CNN. In *Proceedings of the IEEE international conference on computer vision*, pages 2961–2969, 2017.

[21] Kaiming He, Xiangyu Zhang, Shaoqing Ren, and Jian Sun. Deep residual learning for image recognition. In *Proceedings of the IEEE conference on computer vision and pattern recognition*, pages 770–778, 2016.

[22] Shengfeng He, Rynson WH Lau, Wenxi Liu, Zhe Huang, and Qingxiong Yang. Supercnn: A superpixelwise convolutional neural network for salient object detection. *International journal of computer vision*, 115(3):330–344, 2015.

[23] Shihua Huang, Zhichao Lu, Ran Cheng, and Cheng He. Fapn: Feature-aligned pyramid network for dense image prediction. In *Proceedings of the IEEE/CVF International Conference on Computer Vision*, pages 864–873, 2021.

[24] Varun Jampani, Deqing Sun, Ming-Yu Liu, Ming-Hsuan Yang, and Jan Kautz. Superpixel sampling networks. In *Proceedings of the European Conference on Computer Vision (ECCV)*, pages 352–368, 2018.

[25] Tommi Kerola, Jie Li, Atsushi Kanehira, Yasunori Kudo, Alexis Vallet, and Adrien Gaidon. Hierarchical lovász embeddings for proposal-free panoptic segmentation. In *Proceedings of the IEEE/CVF Conference on Computer Vision and Pattern Recognition*, pages 14413–14423, 2021.

[26] Alexander Kirillov, Ross Girshick, Kaiming He, and Piotr Dollár. Panoptic feature pyramid networks. In *Proceedings of the IEEE/CVF Conference on Computer Vision and Pattern Recognition*, pages 6399–6408, 2019.

[27] Alexander Kirillov, Kaiming He, Ross Girshick, Carsten Rother, and Piotr Dollár. Panoptic segmentation. In *Proceedings of the IEEE/CVF Conference on Computer Vision and Pattern Recognition*, pages 9404–9413, 2019.

[28] Alexander Kirillov, Evgeny Levinkov, Bjoern Andres, Bogdan Savchynskyy, and Carsten Rother. Instancecut: from edges to instances with multicut. In *Proceedings of the IEEE Conference on Computer Vision and Pattern Recognition*, pages 5008–5017, 2017.

[29] Shu Kong and Charless C Fowlkes. Recurrent pixel embedding for instance grouping. In *Proceedings of the IEEE Conference on Computer Vision and Pattern Recognition*, pages 9018–9028, 2018.

[30] Xiangtai Li, Ansheng You, Zhen Zhu, Houlong Zhao, Maoke Yang, Kuiyuan Yang, Shaohua Tan, and Yunhai Tong. Semantic flow for fast and accurate scene parsing. In *European Conference on Computer Vision*, pages 775–793. Springer, 2020.

[31] Yanwei Li, Hengshuang Zhao, Xiaojuan Qi, Liwei Wang, Zeming Li, Jian Sun, and Jiaya Jia. Fully convolutional networks for panoptic segmentation. In *Proceedings of the IEEE/CVF Conference on Computer Vision and Pattern Recognition*, pages 214–223, 2021.

[32] Yi Li, Haozhi Qi, Jifeng Dai, Xiangyang Ji, and Yichen Wei. Fully convolutional instance-aware semantic segmentation. In *Proceedings of the IEEE conference on computer vision and pattern recognition*, pages 2359–2367, 2017.

[33] Xiaodan Liang, Yunchao Wei, Xiaohui Shen, Zequn Jie, Jiashi Feng, Liang Lin, and Shuicheng Yan. Reversible recursive instance-level object segmentation. In *Proceedings of the IEEE Conference on Computer Vision and Pattern Recognition*, pages 633–641, 2016.

[34] Tsung-Yi Lin, Piotr Dollár, Ross Girshick, Kaiming He, Bharath Hariharan, and Serge Belongie. Feature pyramid networks for object detection. In *Proceedings of the IEEE conference on computer vision and pattern recognition*, pages 2117–2125, 2017.

[35] Tsung-Yi Lin, Michael Maire, Serge Belongie, James Hays, Pietro Perona, Deva Ramanan, Piotr Dollár, and C Lawrence Zitnick. Microsoft coco: Common objects in context. In *European conference on computer vision*, pages 740–755. Springer, 2014.

[36] Ze Liu, Yutong Lin, Yue Cao, Han Hu, Yixuan Wei, Zheng Zhang, Stephen Lin, and Baining Guo. Swin transformer: Hierarchical vision transformer using shifted windows. In *Proceedings of the IEEE/CVF International Conference on Computer Vision*, pages 10012–10022, 2021.

[37] Jonathan Long, Evan Shelhamer, and Trevor Darrell. Fully convolutional networks for semantic segmentation. In *Proceedings of the IEEE conference on computer vision and pattern recognition*, pages 3431–3440, 2015.

[38] Ilya Loshchilov and Frank Hutter. Decoupled weight decay regularization. *arXiv preprint arXiv:1711.05101*, 2017.

[39] Wenjie Luo, Yujia Li, Raquel Urtasun, and Richard Zemel. Understanding the effective receptive field in deep convolutional neural networks. *Advances in neural information processing systems*, 29, 2016.

[40] Fausto Milletari, Nassir Navab, and Seyed-Ahmad Ahmadi. V-net: Fully convolutional neural networks for volumetric medical image segmentation. In *2016 fourth international conference on 3D vision (3DV)*, pages 565–571. IEEE, 2016.

[41] Davy Neven, Bert De Brabandere, Marc Proesmans, and Luc Van Gool. Instance segmentation by jointly optimizing spatial embeddings and clustering bandwidth. In *Proceedings of the IEEE/CVF Conference on Computer Vision and Pattern Recognition*, pages 8837–8845, 2019.

[42] Adam Paszke, Sam Gross, Francisco Massa, Adam Lerer, James Bradbury, Gregory Chanan, Trevor Killeen, Zeming Lin, Natalia Gimelshein, Luca Antiga, Alban Desmaison, Andreas Kopf, Edward Yang, Zachary DeVito, Martin Raison, Alykhan Tejani, Sasank Chilamkurthy, Benoit Steiner, Lu Fang, Junjie Bai, and Soumith Chintala. Pytorch: An imperative style, high-performance deep learning library. In H. Wallach, H. Larochelle, A. Beygelzimer, F. d'Alché-Buc, E. Fox, and R. Garnett, editors, *Advances in Neural Information Processing Systems 32*, pages 8024–8035. Curran Associates, Inc., 2019.

[43] Pedro O Pinheiro, Tsung-Yi Lin, Ronan Collobert, and Piotr Dollár. Learning to refine object segments. In *European conference on computer vision*, pages 75–91. Springer, 2016.

[44] Zhen Qin, Weixuan Sun, Hui Deng, Dongxu Li, Yunshen Wei, Baohong Lv, Junjie Yan, Lingpeng Kong, and Yiran Zhong. cosformer: Rethinking softmax in attention. *arXiv preprint arXiv:2202.08791*, 2022.

[45] Xiaofeng Ren and Jitendra Malik. Learning a classification model for segmentation. In *Computer Vision, IEEE International Conference on*, volume 2, pages 10–10. IEEE Computer Society, 2003.

[46] Olaf Ronneberger, Philipp Fischer, and Thomas Brox. U-net: Convolutional networks for biomedical image segmentation. In *International Conference on Medical image computing and computer-assisted intervention*, pages 234–241. Springer, 2015.

[47] Zhuoran Shen, Mingyuan Zhang, Haiyu Zhao, Shuai Yi, and Hongsheng Li. Efficient attention: Attention with linear complexities. In *Proceedings of the IEEE/CVF Winter Conference on Applications of Computer Vision*, pages 3531–3539, 2021.

[48] David Stutz, Alexander Hermans, and Bastian Leibe. Superpixels: An evaluation of the state-of-the-art. *Computer Vision and Image Understanding*, 166:1–27, 2018.

[49] Teppei Suzuki. Superpixel segmentation via convolutional neural networks with regularized information maximization. In *ICASSP 2020-2020 IEEE International Conference on Acoustics, Speech and Signal Processing (ICASSP)*, pages 2573–2577. IEEE, 2020.

[50] Teppei Suzuki. Implicit integration of superpixel segmentation into fully convolutional networks. *arXiv preprint arXiv:2103.03435*, 2021.

[51] Teppei Suzuki, Shuichi Akizuki, Naoki Kato, and Yoshimitsu Aoki. Superpixel convolution for segmentation. In *2018 25th IEEE International Conference on Image Processing (ICIP)*, pages 3249–3253. IEEE, 2018.

[52] Shota Takayama, Teppei Suzuki, Yoshimitsu Aoki, Sho Isobe, and Makoto Masuda. Tracking people in dense crowds using supervoxels. In *2016 12th International Conference on Signal-Image Technology Internet-Based Systems (SITIS)*, pages 532–537, 2016.

[53] Jasper RR Uijlings, Koen EA Van De Sande, Theo Gevers, and Arnold WM Smeulders. Selective search for object recognition. *International journal of computer vision*, 104(2):154–171, 2013.

[54] Ashish Vaswani, Prajit Ramachandran, Aravind Srinivas, Niki Parmar, Blake Hechtman, and Jonathon Shlens. Scaling local self-attention for parameter efficient visual backbones. In *Proceedings of the IEEE/CVF Conference on Computer Vision and Pattern Recognition*, pages 12894–12904, 2021.

[55] Ashish Vaswani, Noam Shazeer, Niki Parmar, Jakob Uszkoreit, Llion Jones, Aidan N Gomez, Łukasz Kaiser, and Illia Polosukhin. Attention is all you need. *Advances in neural information processing systems*, 30, 2017.

[56] Huiyu Wang, Yukun Zhu, Hartwig Adam, Alan Yuille, and Liang-Chieh Chen. MaX-DeepLab: End-to-end panoptic segmentation with mask transformers. In *Proceedings of the IEEE/CVF Conference on Computer Vision and Pattern Recognition*, pages 5463–5474, 2021.

[57] Wenhai Wang, Enze Xie, Xiang Li, Deng-Ping Fan, Kaitao Song, Ding Liang, Tong Lu, Ping Luo, and Ling Shao. Pyramid vision transformer: A versatile backbone for dense prediction without convolutions. In *Proceedings of the IEEE/CVF International Conference on Computer Vision*, pages 568–578, 2021.

[58] Xinlong Wang, Tao Kong, Chunhua Shen, Yuning Jiang, and Lei Li. Solo: Segmenting objects by locations. In *European Conference on Computer Vision*, pages 649–665. Springer, 2020.

[59] Xinlong Wang, Rufeng Zhang, Tao Kong, Lei Li, and Chunhua Shen. Solov2: Dynamic and fast instance segmentation. *Advances in Neural information processing systems*, 33:17721–17732, 2020.

[60] Zbigniew Wojna, Vittorio Ferrari, Sergio Guadarrama, Nathan Silberman, Liang-Chieh Chen, Alireza Fathi, and Jasper Uijlings. The devil is in the decoder. In *British Machine Vision Conference 2017, BMVC 2017*, pages 1–13. BMVA Press, 2017.

[61] Enze Xie, Wenhai Wang, Zhiding Yu, Anima Anandkumar, Jose M Alvarez, and Ping Luo. Segformer: Simple and efficient design for semantic segmentation with transformers. *Advances in Neural Information Processing Systems*, 34, 2021.

[62] Yunyang Xiong, Zhanpeng Zeng, Rudrasis Chakraborty, Mingxing Tan, Glenn Fung, Yin Li, and Vikas Singh. Nyströmformer: A nystöm-based algorithm for approximating self-attention. In *Proceedings of the... AAAI Conference on Artificial Intelligence. AAAI Conference on Artificial Intelligence*, volume 35, page 14138. NIH Public Access, 2021.

[63] Yuwen Xiong, Renjie Liao, Hengshuang Zhao, Rui Hu, Min Bai, Ersin Yumer, and Raquel Urtasun. Upsnet: A unified panoptic segmentation network. In *Proceedings of the IEEE/CVF Conference on Computer Vision and Pattern Recognition*, pages 8818–8826, 2019.

[64] Jiarui Xu, Shalini De Mello, Sifei Liu, Wonmin Byeon, Thomas Breuel, Jan Kautz, and Xiaolong Wang. GroupViT: Semantic Segmentation Emerges from Text Supervision. *arXiv preprint arXiv:2202.11094*, 2022.

[65] Fengting Yang, Qian Sun, Hailin Jin, and Zihan Zhou. Superpixel segmentation with fully convolutional networks. In *Proceedings of the IEEE/CVF Conference on Computer Vision and Pattern Recognition*, pages 13964–13973, 2020.

[66] Jian Yao, Marko Boben, Sanja Fidler, and Raquel Urtasun. Real-time coarse-to-fine topologically preserving segmentation. In *Proceedings of the IEEE conference on computer vision and pattern recognition*, pages 2947–2955, 2015.

[67] Fisher Yu and Vladlen Koltun. Multi-scale context aggregation by dilated convolutions. *arXiv preprint arXiv:1511.07122*, 2015.

[68] Wenwei Zhang, Jiangmiao Pang, Kai Chen, and Chen Change Loy. K-Net: Towards unified image segmentation. *Advances in Neural Information Processing Systems*, 34, 2021.

[69] Hengshuang Zhao, Jianping Shi, Xiaojuan Qi, Xiaogang Wang, and Jiaya Jia. Pyramid scene parsing network. In *Proceedings of the IEEE conference on computer vision and pattern recognition*, pages 2881–2890, 2017.

[70] Bolei Zhou, Hang Zhao, Xavier Puig, Tete Xiao, Sanja Fidler, Adela Barriuso, and Antonio Torralba. Semantic understanding of scenes through the ade20k dataset. *International Journal of Computer Vision*, 127(3):302–321, 2019.

[71] Xizhou Zhu, Han Hu, Stephen Lin, and Jifeng Dai. Deformable convnets v2: More deformable, better results. In *Proceedings of the IEEE/CVF Conference on Computer Vision and Pattern Recognition*, pages 9308–9316, 2019.

A Post-processing for the MaskFormer's segmentation head and the relation to the clustering

Let $P \in \Delta^{N_m \times K+1}$ be the $(K+1)$ class probability for masks computed by eq. (4). For a post-processing, we assign a pixel at $j = [h, w]$ to one of the N_m predicted probability-mask pairs via $\arg\max_{i:c_i \neq \Phi} P_{i,c_i} M_{i,j}$, where c_i is the most likely class label, $c_i = \arg\max_{c \in \{1,\dots,K,\Phi\}} P_{i,c}$, for each probability-mask pair i.

The maximization problem in post-processing, $\arg\max_{i:c_i \neq \Phi} P_{i,c_i} M_{i,hw}$, corresponds to the clustering problem, eq. (2). Specifically, $P_{i,c_i} M_{i,j}$ is a similarity between the i-th mask query and the pixel at $j = [h, w]$, and the maximization problem selects the most similar mask. This procedure corresponds to the clustering problem for the pixel with the mask query as a prototype. Thus, we can view MaskFormer's segmentation head as a clustering module.

B Local attention for the clustering module

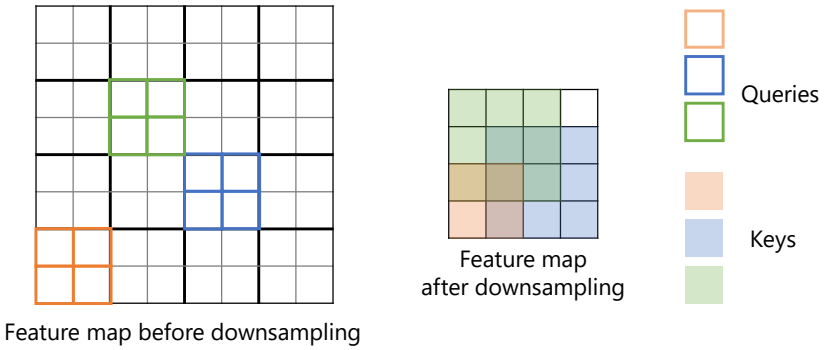

Figure I: Illustration of the local attention.

Pixels in the feature map before downsampling (queries) are groups with pixels in the feature map after downsampling as keys (i.e., cluster prototypes). However, naive computation, eq. (3), is intractable because the complexity is $O(M^2)$, where M denotes the number of pixels. To reduce the complexity, we divide the feature map before downsampling into 2×2 windows (bold lines in Fig. I). The window size is determined by a stride of downsampling. Each window corresponds one-to-one to the pixel in the feature map after downsampling. Then, the attention is computed between each query and the pixel corresponding to the window in which the query belongs and its neighboring pixels. Each color in Fig. I indicates the correspondence between queries and keys for the local attention. As a result, the assignment probability computed in eq. (3) for each pixel has 9-dimension. This procedure is based on a method used in superpixel segmentation[24, 1, 65] that is also a pixel clustering algorithm.

For our clustering module, the local attention implicitly exploits the prior for natural images that are mainly composed of low-frequency components. This is a well-known prior as local smoothness and is widely used in image processing. In our method, we assume that adjacent or close pixels have the same semantics or belong in the same instance.

C Example PyTorch implementation

We show example PyTorch[42] implementation of the soft clustering and the cluster-based decoding. We can easily implement the local attention by using the `unfold` and `einsum` functions.

Listing 1: The proposed soft clustering (eq. (3))

```
import torch
import torch.nn.functional as F


def attention_as_clustering(feat, downsampled_feat, scale):
```

```
    batch_size, emb_dim, height, width = feat.shape
    # get 9 candidate clusters and corresponding pixel features
    candidate_clusters = F.unfold(downsampled_feat, kernel_size=3, padding=1).reshape(
      batch_size, emb_dim, 9, -1)
    feat = F.unfold(feat, kernel_size=2, stride=2).reshape(batch_size, emb_dim, 4, -1)
    # calculate similarities
    similarities = torch.einsum('bkcn,bkpn->bcpn', (candidate_clusters, feat)).reshape(
      batch_size*9, 4, -1)
    similarities = F.fold(similarities, (height, width), kernel_size=2, stride=2).reshape
      (batch_size, 9, height, width)
    # normalize
    soft_assignment = (similarities / scale.abs()).softmax(1)
    return soft_assignment
```

Listing 2: The cluster-based decoding (eq. (5))

```
import torch
import torch.nn.functional as F


def decode(x, A):
    batch_size, _, height, width = A.shape
    n_channels = x.shape[1]
    # get 9 candidate clusters and corresponding assignments
    candidate_clusters = F.unfold(x, kernel_size=3, padding=1).reshape(batch_size,
      n_channels, 9, -1)
    A = F.unfold(A, kernel_size=2, stride=2).reshape(batch_size, 9, 4, -1)
    # decoding
    decoded_features = torch.einsum('bkcn,bcpn->bkpn', (candidate_clusters, A)).reshape(
      batch_size, n_channels * 4, -1)
    decoded_features = F.fold(decoded_features, (height, width), kernel_size=2, stride=2)
    return decoded_features
```

D Detailed experimental setup

We trained models with the Swin-L backbones for the COCO dataset on 4× NVIDIA A100 GPUs and the other models on 2× NVIDIA RTX8000 GPUs. The training protocol is following Mask2Former[11] except for the number of training epochs for HCFormer+. We describe the details as follows.

D.1 Panoptic and instance segmentation on COCO

For HCFormer with the ResNet-50 and Swin-S backbones, we set the number of training epochs and the trainable queries that are fed into the transformer decoder to 50 and 100, respectively. For HCFormer with the Swin-L backbone, these parameters are set to 100 and 200. For HCFormer+, the number of epochs is set to 100 for the ResNet-50 and Swin-S backbones and 200 for the Swin-L backbone, and other parameters are the same as HCFormer. We use an initial learning rate of 0.0001 and a weight decay of 0.05 for all backbones. A learning rate multiplier of 0.1 is applied to the backbone, and we decay the learning rate at 0.9 and 0.95 fractions of the total number of training steps by a factor of 10. We use AdamW optimizer[38] with a batch size of 16. We initialize the scale parameter $s^{(i)}$ with 0.1. For data augmentation, we use the same policy as in Mask2Former[11]. For inference, we use the Mask R-CNN inference setting[20], where we resize an image with shorter side to 800 and longer side up to 1333.

D.2 Semantic segmentation on AD20K and Cityscapes

We use AdamW[38] and the poly learning rate schedule with an initial learning rate of 0.0001 and a weight decay of 0.05. A learning rate multiplier of 0.1 is applied to the backbones. A batch size is set to 16. We initialize the scale parameter $s^{(i)}$ with 0.1. For data augmentation, we use random scale jittering between 0.5 and 2.0, random horizontal flipping, random cropping, and random color jittering. For the ADE20K dataset, if not stated otherwise, we use a crop size of 512×512 and train HCFormer for 160k iterations and HCFormer+ for 320k iterations. For the Cityscapes dataset, we use a crop size of 512×1024 and train HCFormer for 90k iterations and HCFormer+ for 180k iterations. The number of trainable queries is set to 100 for all models and both datasets.

E Additional results

E.1 Per-pixel classification with hierarchical clustering

As described in Sec. 2.2, our hierarchical clustering scheme can be naturally incorporated into per-pixel classification models. Thus, we evaluate the proposed method combined with the per-pixel classification models. As a baseline, we use FCN-32s[34], FPN[34], PSPNet[69], and Deeplabv3[8], and we combine the proposed module with FCN-32s, PSPNet, and Deeplabv3. We refer to the combined models as HC-FCN-32s, HC-PSPNet, and HC-Deeplabv3, respectively. We use ResNet-101[21] as the backbone for all models. Note that PSPNet and Deeplabv3 use dilated convolution[67, 7] in the backbone and their output stride is 8, meaning that the number of downsampling layers in the backbone is 3. HC-PSPNet and HC-Deeplabv3 remove the dilated convolution and use the same backbone architecture as FCN-32s; their output stride is 32. The training protocol is following [69]. We set the crop size for ADE20K to 512×512.

Table I: Evaluation results on semantic segmentation with per-pixel models. The inference time is measured with NVIDIA Quadro RTX8000.

(a) ADE20K

Models	mIoU	Pixel Acc.	msec/image
PSPNet	42.7	80.9	48.7
HC-PSPNet	42.6	80.9	19.0
Deeplabv3	42.7	81.0	62.5
HC-Deeplabv3	42.8	81.1	22.5

(b) Cityscapes

Method	mIoU	Pixel acc.	msec/image
FCN-32s	71.7	94.9	71.7
FPN	75.1	95.8	82.0
HC-FCN-32s	76.1	96.1	87.2
PSPNet	77.7	96.2	298.7
HC-PSPNet	77.6	96.2	88.1
Deeplabv3	78.4	96.3	380.8
HC-Deeplabv3	77.6	96.3	93.9

We show the evaluation results for the validation set in Tab. I. The latency of HC-PSPNet and HC-Deeplabv3 is lower than that of PSPNet and Deeplabv3, and HC-PSPNet shows the comparable result for PSPNet for both datsets. However, mIoU of HC-Deeplabv3 on Cityscapes is lower than that of Deeplabv3. Deeplabv3 uses atrous spatial pyramid pooling (ASPP) that uses several dilated (atrous) convolution layers with different dilation, and the maximum dilation is 24, which corresponds to the convolution with a kernel size of 49. For HC-Deeplabv3, the resolution of the feature map fed into the ASPP layer would be quite low. As a result, HC-Deeplabv3 degrades mIoU from Deeplabv3.

Compared to FCN-32s, HC-FCN-32s significantly improves mIoU because it can preserve detailed information, such as object boundaries, via the clustering module. In addition, HC-FCN-32s shows the superior mIoU than FPN, that is, FCN-32s with the simple pixel decoder, which is also used in MaskFormer[12], while the latency is higher than FPN. This result is consistent with the results of the comparison between HCFormer and MaskFormer.

E.2 Effect of downsampling

In the experiments, we use the deformable convolution v2 (DCNv2)[71] as the downsampling for the ResNet backbone. We verify its effect by comparing the ResNet backbone with and without DCNv2. We train models using the same training protocol for both models with and without DCNv2 (Sec. D.1). Note that the hierarchical level is shown in Fig. II.

We show the evaluation results for COCO[35] in Tab. II. Note that since the downsampling layer is replaced with DCNv2 only for the layers to which the clustering module is attached, both results for the hierarchical level of 0 are the same. DCNv2 significantly improves PQ, especially for hierarchical levels of 2 and 3. The higher the hierarchical level, the more sampling error is accumulated. Thus, the improvement is larger for the higher level.

Note that we do *not* use DCNv2 as downsampling for the transformer-based backbone (Swin-S and Swin-L), and the accuracy of HCFormer with the transformer-based backbone is higher than that of MaskFormer. Thus, the effectiveness of HCFormer is significant, although its accuracy of HCFormer with the CNN-based backbone is almost the same as that of MaskFormer.

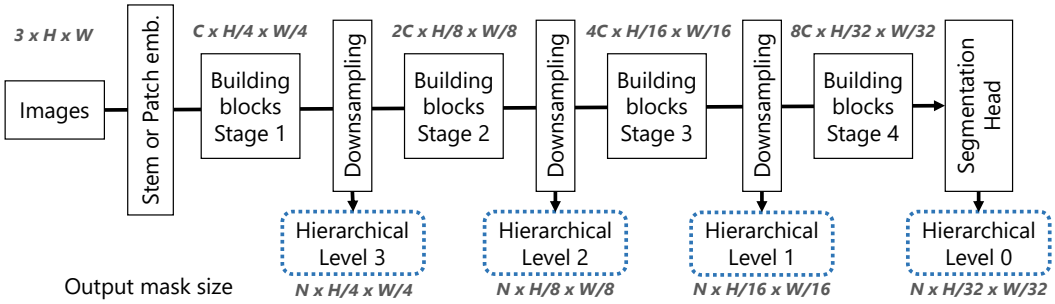

Figure II: Backbone architecture with hierarchical clustering.

Table II: Evaluation results on COCO `val.` with various hierarchical levels.

(a) w/ DCNv2

Hierarchical Level	0	1	2	3
PQ	41.9	45.6	46.7	47.7
FLOPs	82G	83G	84G	87G
#Params	37M	38M	38M	38M

(b) w/o DCNv2

Hierarchical Level	0	1	2	3
PQ	41.9	44.0	44.8	45.3
FLOPs	82G	83G	84G	87G
#Params	37M	38M	38M	38M

E.3 Additional ablation study

We show the additional ablation study. Basically, we use ResNet-50 as a backbone model, except for the result in Tab. VI, and the training protocol is the same as described in Sec. D.

We evaluate HCFormer with the transformer decoder used in MaskFormer[12], although the masked transformer decoder[11] was used in the experiments in the main manuscript. As shown in Tab. III, HCFormer with the standard transformer decoder still outperforms MaskFormer. The difference between HCFormer and MaskFormer in Tab. III is the decoding process. Thus, our hierarchical clustering scheme generates more accurate masks than the pixel decoder, namely the upsampling and then clustering scheme. Moreover, the training iteration for HCFormer is one-third that for MaskFormer. The simplification of the architecture may make optimization easier.

We evaluate HCFormer using various number of trainable queries (Tab. IV). The segmentation accuracy is saturated at about 100 or 150. For memory efficiency, 50 or 100 queries would be preferred.

We evaluate HCFormer with the various hierarchical levels on the semantic segmentation (ADE20K). We verify the improvement of the accuracy on the semantic segmentation, as shown in Tab. V. In addition, we evaluate HCFormer with the Swin-S[36] backbone with various numbers of hierarchical level on COCO[35]. Regardless of the backbone type and dataset, higher hierarchical level leads to higher accuracy.

We evaluate HCFormer with the ResNet-50 backbone with various numbers of transformer decoder layers. MaskFormer[12] reports reasonable semantic segmentation performance (43.0 mIoU on ADE20K) with only one transformer decoder layer. HCFormer with only one transformer decoder layer also shows reasonable results (43.2 mIoU on ADE20K), as shown in Tab. VII. This result is better than the per-pixel classification baselines with ResNet-101[21], such as PSPNet[69] and Deeplabv3[8], as shown in Tab. I. The deeper transformer decoder improves mIoU, and four or eight layers would be sufficient for HCFormer.

E.4 Visualization

We show example results on ADE20K by HCFormer with Swin-L[36] in Fig. III. Basically, the undersegmentation error appears near the boundaries between regions because of ambiguity and downsampling in stem and patch embedding layers of the backbone to which the clustering module is not attached. In the outdoor image (top row), the undersegmentation error appears in the tree region (green region) in the coarser clustering levels, but this would be due to the annotation error. In the indoor image (bottom row), the undersegmentation error appears below the cabinet region (pink region) in all the levels because the pixels in the wall and floor regions are grouped. In addition,

Table III: Evaluation results of HCFormer with the standard transformer decoder used in [6, 12].

method	PQ	FLOPs
MaskFormer[12]	46.5	181G
HCFormer	47.6	97G

Table IV: Evaluation results with various numbers of trainable queries.

#Queries	20	50	100	150	200
COCO (PQ)	42.2	46.3	47.7	47.9	47.9
ADE20K (mIoU)	44.4	45.5	45.5	44.8	44.4
Cityscapes (mIoU)	75.9	75.4	76.7	76.2	76.4

Table V: Evaluation results on ADE20K `val.` with various hierarchical levels.

Hierarchical Level	0	1	2	3
mIoU	42.2	43.4	44.0	45.5
FLOPs	28G	28G	28G	29G
#Params	37M	38M	38M	38M

Table VI: Evaluation results on COCO `val.` with various hierarchical levels for the Swin-S backbone.

Hierarchical Level	0	1	2	3
PQ	47.5	49.7	50.5	50.9
FLOPs	167G	167G	168G	170G
#Params	62M	62M	62M	62M

Table VII: Evaluation results on ADE20K `val.` with various numbers of transformer decoder layers.

#Decoder Layers	1	2	4	8	16
mIoU	43.2	44.4	44.5	45.5	46.1
FLOPs	28G	28G	28G	29G	31G
#Params	27M	29M	32M	38M	51M

HCFormer misclassifies the cabinet and the towel as wall and door, respectively. The backbone model would not recognize their semantics, although it was able to discriminate between pixels in the cabinet and pixels in the wall because the undersegmentation error only appears in their boundaries.

We show example results for COCO panoptic segmentation by HCFormer+ with Swin-L[36] in Fig. IV. HCFormer segments the image well albeit with some misclassification. Thus, to solve such misclassification error, we would need to improve the transformer decoder and/or incorporate stronger backbones.

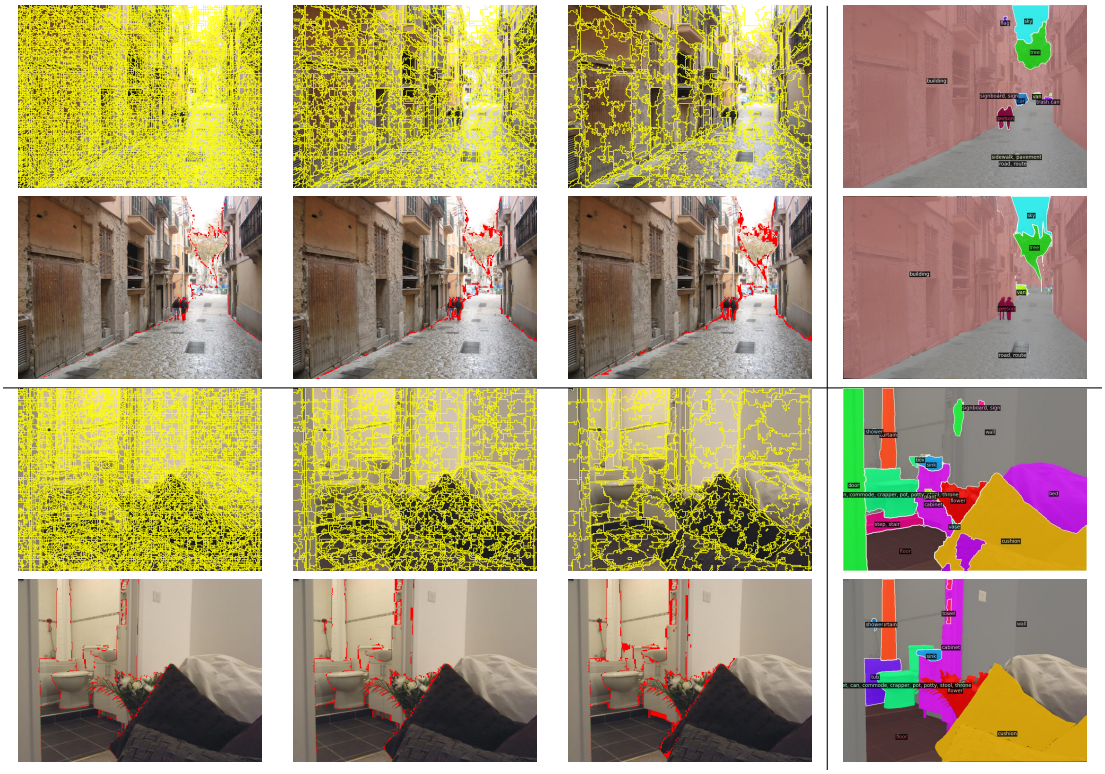

Figure III: Example results on ADE20K. The top row shows the cluster boundaries and predicted masks, and the bottom row shows the undersegmentation error[48] as red regions and the ground-truth label.

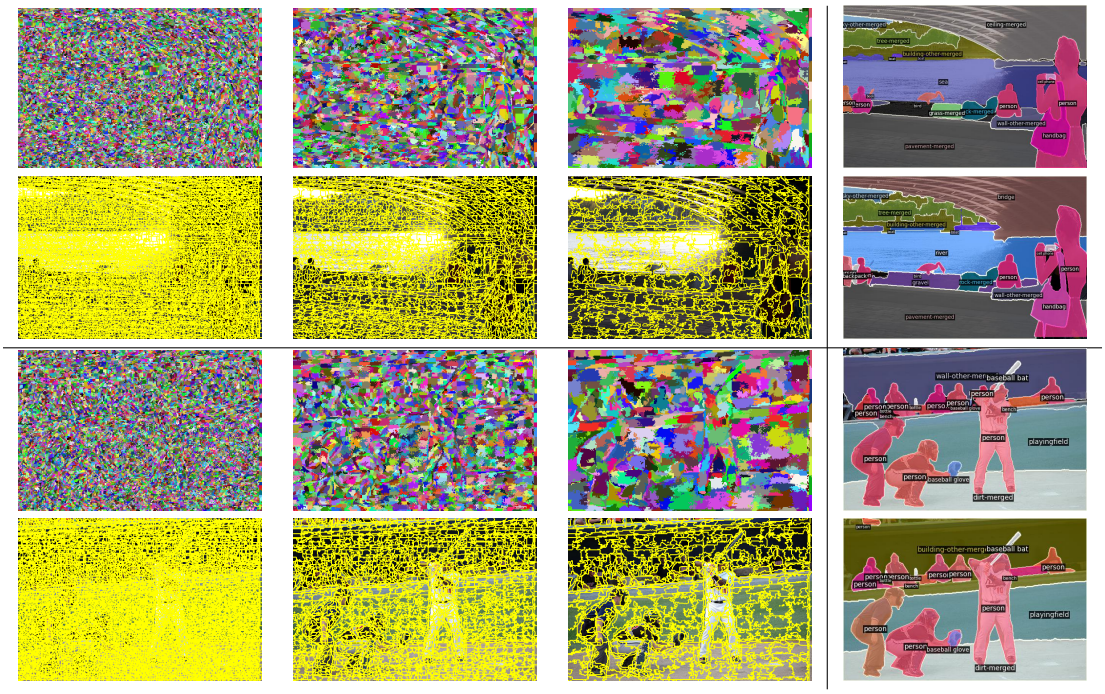

Figure IV: Example results on COCO. The top row shows hierarchical clustering results to which a random color is assigned and prediction, and the bottom row shows cluster boundaries and ground truth.